

## MOST DOUBLE DEGENERATE LOW MASS WHITE DWARF BINARIES MERGE

WARREN R. BROWN<sup>1</sup>, MUKREMIN KILIC<sup>2</sup>, SCOTT J. KENYON<sup>1</sup>, AND A. GIANNINAS<sup>2</sup>

<sup>1</sup>Smithsonian Astrophysical Observatory, 60 Garden St, Cambridge, MA 02138 USA

<sup>2</sup>Homer L. Dodge Department of Physics and Astronomy, University of Oklahoma, 440 W. Brooks St., Norman, OK, 73019 USA

*ApJ accepted*

### ABSTRACT

We estimate the merger rate of double degenerate binaries containing extremely low mass (ELM)  $< 0.3 M_{\odot}$  white dwarfs in the Galaxy. Such white dwarfs are detectable for timescales of 0.1 Gyr – 1 Gyr in the ELM Survey; the binaries they reside in have gravitational wave merger times of 0.001 Gyr – 100 Gyr. To explain the observed distribution requires that most ELM white dwarf binary progenitors detach from the common envelope phase with  $< 1$  hr orbital periods. We calculate the local space density of ELM white dwarf binaries and estimate a merger rate of  $3 \times 10^{-3} \text{ yr}^{-1}$  over the entire disk of the Milky Way; the merger rate in the halo is 10 times smaller. The ELM white dwarf binary merger rate exceeds by a factor of 40 the formation rate of stable mass transfer AM CVn binaries, marginally exceeds the rate of underluminous supernovae, and is identical to the formation rate of R CrB stars. On this basis, we conclude that ELM white dwarf binaries can be the progenitors of all observed AM CVn and possibly underluminous supernovae, however the majority of He+CO white dwarf binaries go through unstable mass transfer and merge, e.g. into single massive  $\sim 1 M_{\odot}$  white dwarfs.

*Subject headings:* binaries: close — Galaxy: stellar content — white dwarfs

### 1. INTRODUCTION

Double degenerate white dwarf (WD) binaries with orbital periods less than about 6 hours will merge within a Hubble time due to energy and angular momentum loss from gravitational wave radiation. Pairs of normal,  $0.6 M_{\odot}$  CO WDs are rarely found in such compact binaries, however. The Supernovae Progenitor Survey obtained precision radial velocities for 1,014 nearby WDs and identified 5 double degenerate binaries that will merge within a Hubble time (Napiwotzki et al. 2007). This result is consistent with simulations: binary population synthesis models predict that most of the WD+WD mergers in the Milky Way are low mass He+He WD and He+CO WD binaries (Iben 1990; Han 1998; Nelemans et al. 2001). The reason is that helium-core  $\lesssim 0.3 M_{\odot}$  ELM WDs form out of common envelope evolution in ultra-compact binaries (Marsh et al. 1995), exactly the type of binaries that quickly merge.

Over the past five years, our targeted survey for ELM WDs has uncovered 76 short period  $P \leq 1$  day double degenerate binaries containing an ELM WD (Brown et al. 2010, 2012b, 2013, 2016; Kilic et al. 2010b, 2011a, 2012; Gianninas et al. 2015). The success of the ELM Survey in finding these binaries is explained in part by the long evolutionary times of the ELM WDs. ELM WDs are predicted to have thick H envelopes with residual shell burning that cause them to remain hot  $T_{\text{eff}} > 8,000$  K and luminous  $M_g < 9$  mag for many Gyr (Sarna et al. 2000; Panei et al. 2007; Althaus et al. 2013; Istrate et al. 2014). The gravitational wave merger times of the observed binaries, on the other hand, are as short as 1 Myr (Brown et al. 2011b).

Our ELM Survey is now large enough and complete enough that we can use the distribution of objects to infer the merger rate of ELM WD binaries throughout the

Milky Way. We made an early attempt at this calculation using the first 12 ELM WDs found in the original Hypervelocity Star Survey (Brown et al. 2011a). This first sample was based on WDs identified by visual inspection; stellar atmosphere fits subsequently uncovered additional ELM WDs in the Hypervelocity Star Survey (Brown et al. 2013). More importantly, our subsequent discoveries include four systems with orbital periods  $< 40$  min and with merger times  $< 27$  Myr (Brown et al. 2011b; Kilic et al. 2011b,c, 2014a). The existence of such short merger-time systems implies that ELM WD binary mergers are more frequent than previously thought.

An outstanding question is what happens when ELM WD binaries merge. There are at least three possible outcomes: 1) a long-lived stable mass-transfer binary, 2) an explosion, and 3) a merger into a single massive WD (e.g., Webbink 1984; Iben 1990; Kilic et al. 2010b). The three outcomes depend on the stability of mass transfer and thus on the mass ratio of the donor and accretor, however there are many complications (e.g., Marsh et al. 2004; Nelson et al. 2004; Kaplan et al. 2012). For reference, the average ELM WD binary in our sample has a mass ratio of about  $M_{\text{donor}}:M_{\text{accretor}} = 1:4$  and total mass of about  $1 M_{\odot}$  (Andrews et al. 2014; Brown et al. 2016).

Kremer et al. (2015) argue that essentially all the observed ELM WD binaries will evolve into stable mass-transfer configurations, binaries in which helium mass transfer can proceed stably for billions of years. Observationally, long-lived stable helium mass-transfer binaries will appear as AM Canum Venaticorum (AM CVn) systems (Warner 1995; Solheim 2010).

Theoretical models suggest that helium mass transfer may lead to a series of thermonuclear flashes, the last of which may result in an underluminous explosion dubbed a supernova “.Ia” (Bildsten et al. 2007; Shen & Bildsten 2009; Waldman et al. 2011). However, models of ELM

WD binaries that are probable AM CVn progenitors find that the conditions for detonation may never develop (Piersanti et al. 2015). The implication is that most ELM WD binaries will end up as long-lived AM CVn systems.

Alternatively, the result may be a merger. If the initial binary mass ratio is  $M_{\text{donor}}/M_{\text{accretor}} > 2/3$ , or if the initial hydrogen mass transfer rate is super-Eddington, a common envelope may form and cause the two WDs to quickly merge into a single massive WD (Webbink 1984; Han & Webbink 1999; Dan et al. 2011; Shen 2015). Observationally, the merger event should form a single object and ignite nuclear burning, appearing as an extreme helium star, including an R CrB star (Paczynski 1971; Webbink 1984; Saio & Jeffery 2002), or He-rich sdO star (Heber et al. 2008). We cannot wait long enough to observe the outcome of an ELM WD binary merger, however we can constrain the outcome by considering the formation rates of AM CVn, underluminous supernovae, and R CrB.

We begin this paper by presenting a clean sample of ELM WD binaries. We divide the sample into disk (63%) and halo (37%) objects on the basis of kinematics and spatial position, and then derive the local space density of disk and halo ELM WD binaries using standard Galactic stellar density models. We estimate merger rates in two ways: by correcting the observed sample for systems that have cooled or merged, and by forward modeling to match the observed distributions. We conclude that the vast majority of ELM WD binaries must form at short  $< 1$  hr orbital periods to explain the observed distribution of ELM WD binaries. We compare the estimated ELM WD binary merger rate with the formation rates of AM CVn systems, underluminous supernovae, and R CrB stars, and conclude that the rates favor non-explosive merger events.

## 2. MODEL INPUT

### 2.1. Clean Sample

ELM Survey targets were selected by de-reddened  $g$ -band magnitudes ( $15 < g_0 < 20$  mag) and by color. Brown et al. (2012a,b) publish the exact color selection, which was designed to target A- and B-type stars with surface gravities between normal main sequence stars with  $\log g \simeq 4$  and normal hydrogen atmosphere WDs with  $\log g \simeq 8$ . Our observing strategy was to acquire a spectrum of each color-selected target, identify its nature, and then re-observe each  $5 \lesssim \log g \lesssim 7$  ELM WD candidate until we constrain its orbital solution.

We define a clean set of ELM WD binaries from the ELM Survey by first restricting the sample to those binaries with  $k > 75 \text{ km s}^{-1}$ . Sensitivity tests demonstrate that our multi-epoch spectroscopy should detect 95% of binary systems with semi-amplitude  $k = 75 \text{ km s}^{-1}$  and 99% of binary systems with  $k = 100 \text{ km s}^{-1}$  out to  $P = 2$  day orbital periods (Brown et al. 2016).

Next, we restrict the sample to those objects with  $4.85 < \log g < 7.15$ , a range over which ELM Survey follow-up observations are 95% complete. The ELM Survey color selection in  $(g - r)$  provides a built-in temperature selection of  $8,000 \text{ K} < T_{\text{eff}} < 22,000 \text{ K}$ .

Finally, we remove the two ELM WDs that were not drawn from the Sloan Digital Sky Survey (SDSS) photo-

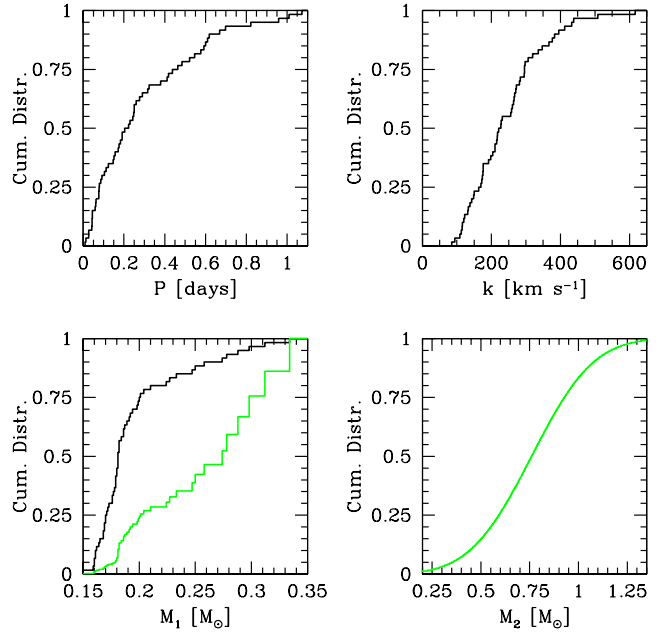


FIG. 1.— Orbital parameter distributions for the clean sample of ELM WD binaries. Orbital period  $P$  and semi-amplitude  $k$  are directly measured. ELM WD mass  $M_1$  is derived from spectroscopic  $T_{\text{eff}}$  and  $\log g$  measurements using Althaus et al. (2013) models; the green line shows the  $M_1$  distribution scaled by the inverse of evolutionary time. Secondary mass  $M_2$  is inferred from the observations (Brown et al. 2016).

metric catalog: NLTT 11748 (Kilic et al. 2010a) and the LAMOST object J0308+5140 (Gianninas et al. 2015). Taken together, these cuts leave us with a clean sample of 60 ELM WD binaries in a well-defined footprint of sky.

We present the clean sample in Table 1 sorted by orbital period. Brown et al. (2016) estimate that this ELM WD sample is 60% complete, given the number of ELM WD candidates that have unknown or poorly constrained orbital parameters. We will thus correct all relevant quantities in this paper assuming a 60% completeness.

### 2.2. White Dwarf Parameters

We adopt the ELM WD masses and luminosities reported in Brown et al. (2016). These parameters were derived by comparing spectroscopic  $T_{\text{eff}}$  and  $\log g$  measurements to the ELM WD evolutionary models of Althaus et al. (2013). A notable feature of the models is that  $\lesssim 0.18 M_{\odot}$  ELM WDs evolve relatively slowly due to residual burning in the hydrogen envelopes, while  $\gtrsim 0.18 M_{\odot}$  ELM WDs evolve more quickly due to unstable hydrogen shell flashes. The ELM WD models follow standard WD mass-radius relations except during these moments of unstable hydrogen shell burning, when the effective radius of the ELM WD is inflated.

Quantitatively, the median observed ELM WD in our clean sample has mass  $M_1 = 0.18 M_{\odot}$ , absolute magnitude  $M_g = +8.5$ , apparent magnitude  $g_0 = 18.5$ , and heliocentric distance  $r = 1.0$  kpc. The SDSS covers a high Galactic latitude region of sky; the median object has latitude  $b = 45^\circ$  and vertical distance above the Galactic plane  $Z = 0.7$  kpc.

We include the ELM WD masses  $M_1$  in Table 1. The

$M_1$  uncertainties are derived by propagating  $T_{\text{eff}}$  and  $\log g$  errors through the tracks and then adding  $0.01 M_{\odot}$  in quadrature, motivated by the comparison with Istrate et al. (2014) models. The Istrate et al. (2014) models yield mass and luminosity estimates that agree to within  $\pm 6\%$  of the Althaus et al. (2013) models, however they have much longer evolutionary times due to the absence of gravitational settling in the stellar atmospheres calculations. We will discuss evolutionary times in more detail below.

Figure 1 shows the cumulative distribution of ELM WD masses. In principle, our surface gravity selection should correspond to uniform selection in mass. In practice, most of the ELM WDs we observe are clumped around  $0.18 M_{\odot}$ . The discontinuity in the mass distribution is good evidence that, as predicted, shell flashes cause  $\gtrsim 0.18 M_{\odot}$  ELM WDs to evolve much more quickly than their lower mass brethren. If we scale each object by the inverse of its evolution time, such that more rapidly evolving ELM WDs contribute a greater fraction of the sample, then we obtain a more uniform  $M_1$  distribution as seen in Figure 1.

### 2.3. Binary Orbital Parameters

We adopt the ELM WD binary orbital parameters reported in Brown et al. (2016). We include the measured semi-amplitude  $k$  and orbital period  $P$  in Table 1, and plot their cumulative distributions in Figure 1. Orbital periods have a lognormal distribution and a median value of 0.21 days.

ELM WDs dominate the light of the binary systems because the ELM WDs are larger in radius and hotter in temperature than their older, more massive WD companions. We thus observe single-lined spectroscopic binaries, and must rely on the binary mass function to constrain the mass of the unseen companions. The binary mass function,

$$\frac{Pk^3}{2\pi G} = \frac{(M_2 \sin i)^3}{(M_1 + M_2)^2}, \quad (1)$$

relates  $M_2$  to the measured and derived parameters  $P$ ,  $k$ , and  $M_1$  plus the inclination  $i$ . We do not know the inclination of individual binaries (unless there are eclipses), however we know that the binaries were selected by color. Thus we can assume that the distribution of inclination is random in  $\sin i$  and solve for the underlying distribution of  $M_2$ . Brown et al. (2016) show that the best fit to the data comes from a normal distribution of  $M_2$  with mean  $0.76 M_{\odot}$  and standard deviation  $0.25 M_{\odot}$  (see Figure 1). Andrews et al. (2014) and Boffin (2015) find essentially the same result using different techniques and an earlier version of the ELM Survey data. Table 1 includes the estimated  $M_2$  for each ELM WD binary given any available inclination constraint; we report the median value of  $M_2$  along with the 0.1587 and 0.8413 percentile values of the  $M_2$  distribution.

### 2.4. Galactic Stellar Density Models

We make use of two Galactic stellar density models in this paper: those of Jurić et al. (2008) and Nelemans et al. (2001). We will use these Galactic stellar density models to derive the local space density of ELM WD binaries, and then to infer the population of ELM WD binaries over the entire Milky Way.

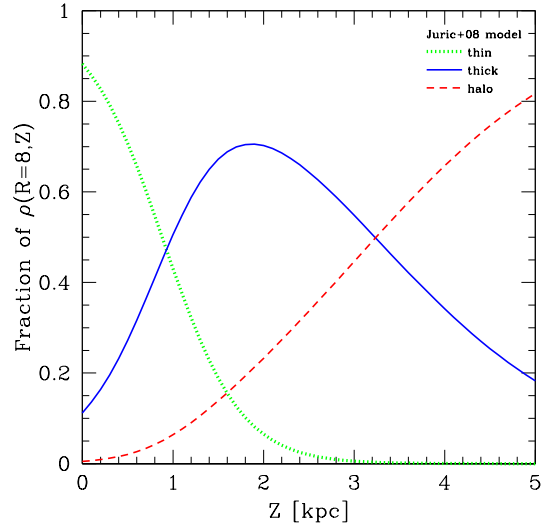


FIG. 2.— Galactic stellar density  $\rho(R, Z)$  versus height above the disk  $Z$  calculated at  $R = 8$  kpc: the thin disk dominates  $Z < 1$  kpc (green dotted line), the thick disk dominates  $Z \sim 2$  kpc (blue solid line), and the halo dominates  $Z > 3$  kpc in the Jurić et al. (2008) model.

Jurić et al. (2008) derive a stellar density model using star counts from SDSS, stars that share the same footprint of sky as the ELM WD binaries. Jurić et al. (2008) formulate the stellar density model with an exponential distribution for the thin- and thick-disk, and a two-axial power-law distribution for the halo:

$$\rho(R, Z)_{\text{thin}} = \rho(R_{\odot}, 0) \exp\left(-\frac{R-R_{\odot}}{2.6} - \frac{|Z+Z_{\odot}|}{0.3}\right) \quad (2)$$

$$\rho(R, Z)_{\text{thick}} = 0.12\rho(R_{\odot}, 0) \exp\left(-\frac{R-R_{\odot}}{3.6} - \frac{|Z+Z_{\odot}|}{0.9}\right) \quad (3)$$

$$\rho(R, Z)_{\text{halo}} = 0.0051\rho(R_{\odot}, 0) \left(\frac{R_{\odot}}{\sqrt{R^2+(Z/0.64)^2}}\right)^{2.77}, \quad (4)$$

where  $R$  and  $Z$  are the Galactocentric cylindrical radial and vertical distances, respectively, in units of kpc, and  $\rho(R, Z)$  is in units of  $\text{kpc}^{-3}$ . We use the Jurić et al. (2008) bias-corrected model parameters, and assume that the Sun is located at  $(R_{\odot}, Z_{\odot}) = (8, 0.025)$  kpc.

Figure 2 plots the fraction of thin disk, thick disk, and halo stars as a function of  $Z$  in the Jurić et al. (2008) stellar density model, calculated at the solar position  $R_{\odot} = 8$  kpc. This fiducial slice illustrates that thin disk stars should dominate at  $|Z| < 1$  kpc, thick disk stars should dominate at  $|Z| \sim 2$  kpc, and halo stars should dominate at  $|Z| > 3$  kpc. The observations sample  $R$  and  $Z$  in a more complicated way than this simple slice, however.

Second, we consider the Nelemans et al. (2001) disk model commonly used in AM CVn studies:

$$\rho(R, Z)_{\text{thin}} = 0.98\rho(R_{\odot}, 0) \exp\left(-\frac{R-R_{\odot}}{2.5}\right) \text{sech}\left(\frac{Z+Z_{\odot}}{0.3}\right)^2 \quad (5)$$

$$\rho(R, Z)_{\text{thick}} = 0.02\rho(R_{\odot}, 0) \exp\left(-\frac{R-R_{\odot}}{2.5}\right) \text{sech}\left(\frac{Z+Z_{\odot}}{1.25}\right)^2 \quad (6)$$

The major difference with respect to the Jurić et al. (2008) model is the use of  $\text{sech}(Z)^2$ , which declines more quickly than an exponential, and a shorter radial scale length. The scale length and scale heights used by

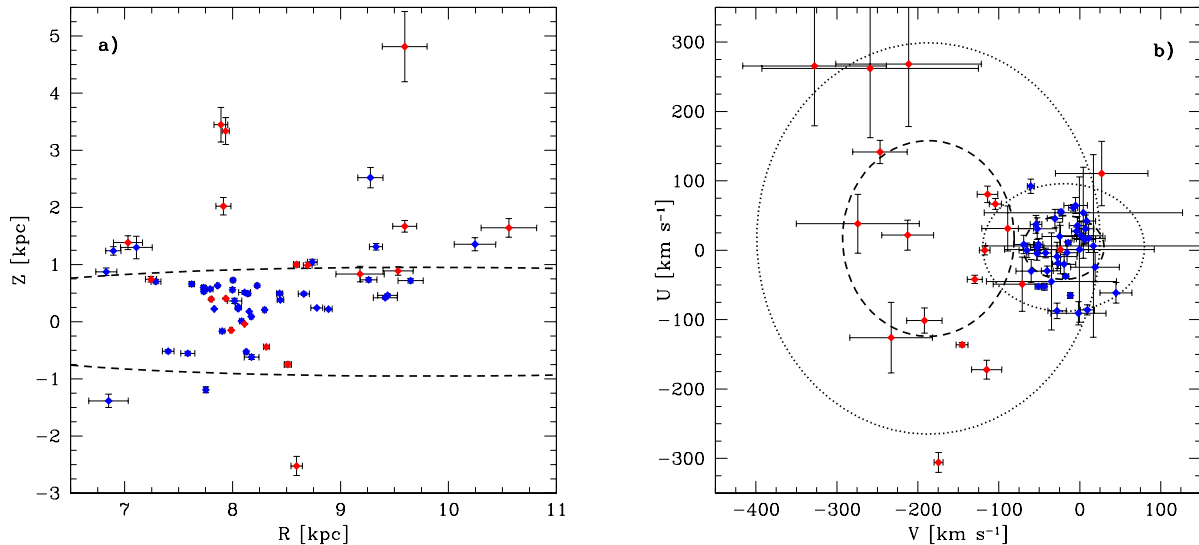


FIG. 3.— a) Spatial distribution of the clean sample of ELM WD binaries plotted in Galactic cylindrical coordinates  $R$  and  $Z$ . Dashed lines indicate where the ratio of disk and halo densities are normalized to 1 for our disk/halo classification scheme. Disk objects are marked blue; halo objects red. b) Velocity distribution of the clean sample, plotted in Galactic cartesian velocity components  $U$  (in the direction of the Galactic center) and  $V$  (in the direction of rotation). For comparison are the  $1\sigma$  (dashed) and  $2\sigma$  (dotted) velocity dispersion thresholds for stellar thick disk and halo populations. Symbols same as in a).

Nelemans et al. (2001) originate from earlier star count studies summarized by Sackett (1997); here, we adopt the thick disk scale height used by Roelofs et al. (2007a). Using this disk model allows us to compare with past AM CVn studies and contrast with the Jurić et al. (2008) disk model.

### 2.5. Disk / Halo Classification

Distinguishing between disk and halo ELM WD binaries is important for our space density and merger rate analysis. We will henceforth use the term “disk” to refer to any object in the thin or thick disk,  $\rho_{\text{disk}} = \rho_{\text{thin}} + \rho_{\text{thick}}$ . It is difficult for our observations to distinguish between thin and thick disk objects, however halo objects stand out by their motion. Some of the first ELM WD binary discoveries had large  $>200 \text{ km s}^{-1}$  systemic radial velocities, a strong indication that they belong to the halo (Kilic et al. 2010b; Brown et al. 2011a). We thus base our initial disk/halo classifications on kinematics.

Gianninas et al. (2015) combine SDSS+USNO-B proper motions (Munn et al. 2004) with ELM Survey distance estimates and radial velocities to calculate  $(U, V, W)$  space velocities for the ELM WD binaries. Gianninas et al. (2015) then determine disk/halo membership on the basis of the Mahalanobis distance, or the number of standard deviations, between an ELM WD space velocity and the velocity ellipsoids of the thick disk and halo,

$$D_m = \sqrt{\frac{(U - \langle U \rangle)^2}{\sigma_U^2} + \frac{(V - \langle V \rangle)^2}{\sigma_V^2} + \frac{(W - \langle W \rangle)^2}{\sigma_W^2}} \quad (7)$$

where  $(\langle U \rangle, \langle V \rangle, \langle W \rangle)$  are the mean velocities and  $(\sigma_U, \sigma_V, \sigma_W)$  are the velocity dispersions of the thick disk or halo. We use the velocity ellipsoid values from Chiba & Beers (2000). A purely kinematic classification suffers some ambiguity, however. As seen in Figure

11 of Gianninas et al. (2015), there is an overdensity of halo classifications in the disk/halo overlap region around  $V = -50 \text{ km s}^{-1}$ , only seen in that one location of the velocity ellipsoid. This overdensity is more naturally explained as disk objects that happen to be above the  $1\sigma$  thick disk threshold and that are erroneously assigned to the halo.

We thus introduce an additional consideration – spatial location – to the selection criteria. Because we want to prevent extraneous halo classifications in the disk-dominated region of the survey, we will require objects closer to the disk plane to need more divergent kinematics to be classified as halo objects. Specifically, we multiply the ratio of Mahalanobis kinematic distances in Equation 7 by the ratio of thick disk to halo space densities. We normalize the ratio of densities to one at the thick disk scale height 0.9 kpc (see dashed line in Figure 3) to make this a relative weighting that varies by about a factor of  $e$  over the sample.

$$D = \frac{D_m(U, V, W)_{\text{thick}}}{D_m(U, V, W)_{\text{halo}}} \times \frac{\rho(R_\odot, 0.9)_{\text{thick}}}{\rho(R, Z)_{\text{thick}}} \frac{\rho(R, Z)_{\text{halo}}}{\rho(R_\odot, 0.9)_{\text{halo}}}, \quad (8)$$

where disk objects have  $D < 1$  and halo objects have  $D > 1$ . Adding the spatial consideration changes 10% of the classifications in the clean sample from halo to disk compared to the purely kinematic criteria, and eliminates the overdensity of halo classifications clumped around  $V = -50 \text{ km s}^{-1}$ .

Because the clean sample contains objects not published in Gianninas et al. (2015), we search for SDSS+USNO-B proper motions for all of the ELM WD binaries presented here. Other proper motion catalogs with brighter limiting magnitudes are not useful because our sample contains faint objects. Five of the  $g \simeq 20$  mag ELM WD binaries have no published proper motion in any catalog. For these five objects we assume a proper motion of zero and depend solely on radial velocity; their

space velocity can only be larger. Applying Equation 8 to the clean sample yields 38 (63%) disk objects and 22 (37%) halo objects. We record the classifications in Table 1 with  $\text{disk}=1$  for disk objects and  $\text{disk}=0$  for halo objects.

### 2.6. Gravitational Wave Merger Timescale

The orbits of ELM WD binaries are shrinking due to gravitational wave radiation. The change in orbital period is observed in the ELM WD binary J0651 (Hermes et al. 2012b). The gravitational wave merger timescale of a binary is

$$\tau = 47925 \frac{(M_1 + M_2)^{1/3}}{M_1 M_2} P^{8/3} \text{ Myr} \quad (9)$$

where the masses are in  $M_\odot$ , the period  $P$  is in days, and the time  $\tau$  is in Myr (Kraft et al. 1962). Note that the merger time depends much more strongly on orbital period than on mass. The range of ELM WD binary mass is also quite limited compared to the range of period. For the average ELM WD binary,  $M_1 + M_2 = 1.01 \pm 0.15 M_\odot$ , the merger time at the median  $P = 0.21$  day is  $\tau = 5$  Gyr.

For each ELM WD binary, we derive the statistical distribution of  $\tau$  from its measured  $P$  and the derived  $M_1$  value and  $M_2$  distribution. We note that edge-on orbits with  $\sin i = 1$  provide a minimum  $M_2$  and a maximum  $\tau$  that cannot be exceeded. We report the median  $\tau$  for each binary in Table 1, along with the 0.1587 and 0.8413 percentile values of the distribution.

The merger times in the clean sample span 1 Myr to over 100 Gyr. This factor of 100,000 in  $\tau$  has important implications. Because the merger rate of ELM WD binaries is essentially a harmonic mean of the merger times, the shortest merger time systems are the most important for the merger rate calculation. Physically, to observe one  $\tau = 1$  Myr system implies that many more such systems must have existed over the  $\sim 1$  Gyr evolutionary time over which our survey can detect an ELM WD. Conversely,  $\tau > 13$  Gyr systems exist longer than the age of the Universe, thus we should observe all of the ones that are detectable.

Merger times are strongly linked to orbital period, thus the distribution of merger times that we observe also has implications for the initial period distribution of the ELM WD binaries. If ELM WDs continuously detach from the common envelope phase at 6 hr periods, for example, half of the clean sample should have  $P = 5\text{--}6$  hr and zero should have  $P < 1$  hr. The fact that we observe the *same* number of objects with  $P = 5\text{--}6$  hr as with  $P < 1$  hr implies that a large fraction of ELM WD binaries form at short orbital periods; to observe  $P < 1$  hr systems requires that they are constantly replenished. We will investigate this point further below.

### 2.7. ELM WD Evolutionary Timescales

WDs cool and fade with time. As mentioned before, ELM WDs remain relatively luminous over Gyr timescales because of residual hydrogen shell burning in the WD atmospheres. The timescale relevant to this paper, however, is the amount of time an ELM WD spends cooling through our color selection region. We quantify this time  $t_{\text{obs}}$  as follows.

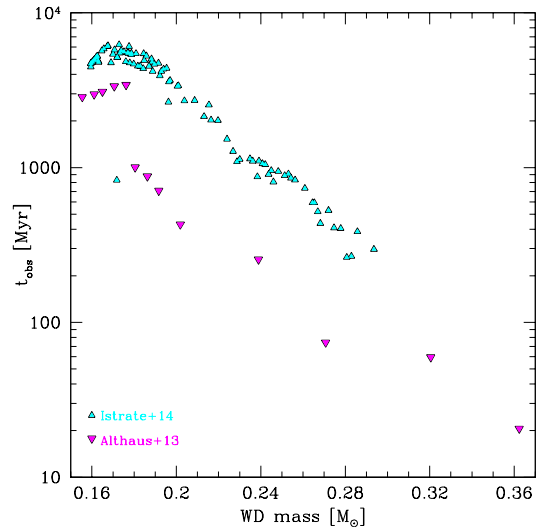


FIG. 4.— Timescale  $t_{\text{obs}}$  that Istrate et al. (2014, cyan) and Althaus et al. (2013, magenta) ELM WD evolutionary tracks would be observed in our color selection region. The break in  $t_{\text{obs}}$  around  $0.18 M_\odot$  is due to the on-set of hydrogen shell flashes in the models.

For each ELM WD evolutionary track, we apply our photometric errors to the synthetic colors at each time step in the track and use a Monte Carlo calculation to estimate what fraction of simulated observations would fall in our color selection region. The evolutionary tracks contain between 2,000 to 50,000 time steps and 3 Gyr to 20 Gyr time spans, with an average time step of 1 Myr in the temperature range sampled by our color selection region. The sum of the time steps multiplied by the fractions in our color selection region equals  $t_{\text{obs}}$ , the time a WD on a given track could be observed in our survey.

The values of  $t_{\text{obs}}$  are plotted in Figure 4 for both Althaus et al. (2013) and Istrate et al. (2014) tracks. The discontinuity in  $t_{\text{obs}}$  around  $0.18 M_\odot$  is due to the onset of hydrogen shell flashes in the models. Notably, Istrate et al. (2014) tracks have  $t_{\text{obs}}$  values that are systematically  $\simeq 5$  times longer than the  $t_{\text{obs}}$  values of the Althaus et al. (2013) tracks. This is likely explained by the absence of gravitational settling in the Istrate et al. (2014) models. We adopt the Althaus et al. (2013) values in this paper.

Given the  $t_{\text{obs}}$  of the models, we estimate  $t_{\text{obs}}$  for each ELM WD by interpolating its measured  $T_{\text{eff}}$  and  $\log g$  with its errors through the tracks. We include the results in Table 1. As before, we report the median  $t_{\text{obs}}$ , with the upper and lower uncertainties being the 0.1587 and 0.8413 percentile values of the distribution. All  $\leq 0.18 M_\odot$  tracks in the Althaus et al. (2013) models have  $t_{\text{obs}} = 3$  Gyr, and so there is no range to report for the lowest mass ELM WDs in the clean sample.

One implication of the  $t_{\text{obs}} = 3$  Gyr timescale is that many of the ELM WD binaries we observe represent an integral of the population over the past few Gyr. ELM WD binaries with  $t_{\text{obs}} < \tau$  must remain visible for the full amount of  $t_{\text{obs}}$ ; they will cool out of the survey before they have time to merge. This statement applies to ELM WD binaries with approximately  $P > 0.18$  day periods, about 57% of the clean sample.

ELM WD binaries with  $t_{\text{obs}} > \tau$ , on the other hand,

represent a snapshot of the population. To observe a  $t_{obs} > \tau$  binary requires that it form with  $P < 0.23$  day and evolve over  $t_{obs}$  to the period we observe today; binaries formed with  $P < 0.18$  day will merge before they reach  $t_{obs}$ , which means we are lucky to observe them at all. ELM WD effective temperatures corroborate this view: if the ELM WD binaries merge before they have time to cool out of the survey, they must be systematically younger and hotter than the other ELM WDs in the survey. In the clean sample,  $P < 0.1$  day binaries have median  $T_{eff} = 16,400$  K while  $P > 0.1$  day binaries have median  $T_{eff} = 11,100$  K. The Anderson-Darling test gives a p-value of less than 0.0001 that the two  $T_{eff}$  distributions are drawn from the same parent distribution (see also Gianninas et al. 2015). The significant difference in temperature means short-period ELM WD binaries merge before they have time to cool; to see the sample that we observe implies that many more short-period ELM WDs must have formed over the past few Gyr.

### 2.8. Roche Lobe Radius

The Roche lobe radius is the effective radius at which an object fills its gravitational equipotential and begins transferring mass to its companion. ELM WDs are always the donor stars in our binaries, because, being degenerate objects, ELM WDs have larger radii than normal WDs (and also neutron stars) of higher mass. An ELM WD will begin mass transfer when its radius exceeds the effective Roche lobe radius  $R_L$ ,

$$\frac{R_L}{A} = \frac{0.49q^{2/3}}{0.6q^{2/3} + \ln(1 + q^{1/3})}, \quad (10)$$

where  $A$  is the orbital separation and  $q = M_{ELM}/M_2$  is the mass ratio (Eggleton 1983). Quantitatively, ELM WDs with  $\log g = 6.5$  have  $0.04 R_\odot$  radii that will exceed  $R_L$  at 10 min orbital periods, periods at which  $\tau \simeq 0.6$  Myr. The gravitational wave merger time is thus broadly consistent with the time at which mass transfer will begin for these objects. This is not true for the lowest surface gravity ELM WDs, however. ELM WDs with  $\log g = 5.5$  have  $0.13 R_\odot$  radii that exceed  $R_L$  at 60 min orbital periods, periods at which  $\tau \simeq 60$  Myr. The time of merger thus depends on the time evolution of ELM WD radii and Roche lobe radii. We consider both  $\tau$  and  $R_L = R_{ELM}$  as merger conditions in our calculations below.

## 3. MERGER RATE ANALYSIS

### 3.1. Space Density of ELM WD Binaries

The first step in estimating the merger rate of ELM WD binaries in the Milky Way is to derive their local space density. To be clear, we are not deriving the local space density of all WDs or all ELM WDs, but the density of our clean sample of ELM WD binaries relevant to the merger rate calculation. The total number of WD binaries can only be larger.

Our approach is to use the modified  $1/V_{max}$  method (Schmidt 1975) commonly used in WD studies (e.g. Rebassa-Mansergas et al. 2015). Stars in the Galaxy are not distributed isotropically in a sphere, but are distributed mostly in a disk. Thus the standard approach is to scale the maximum volume  $V_{max}$  over which each

WD can be observed by a Galactic stellar density model,

$$V_{max} = \int_l \int_b \int_r \frac{\rho(R, Z)}{\rho(R_\odot, 0)} dl \cos b db r^2 dr, \quad (11)$$

where  $l$  is Galactic longitude,  $b$  is Galactic latitude,  $r$  is heliocentric distance. The stellar density model  $\rho(R, Z)$  depends on  $R$  and  $Z$  which can be derived from  $l$ ,  $b$ , and  $r$ . As a practical matter, we integrate the volume for each WD numerically. The volume depends on both our survey apparent magnitude limits  $m_{lim}$  and the SDSS imaging footprint, which is a complicated function of  $l$  and  $b$ . We determine  $l$  and  $b$  coverage from the SDSS stripe definition catalog, clipped by our reddening limit  $E(B - V) < 0.1$ . We observe ELM WDs of different absolute magnitude  $M_g$  to different depths  $r_{lim} = 10^{(m_{lim} - M_g)/5 - 2}$  (kpc), where  $m_{lim} = 15$  and  $20$ . The local space density is then the sum of  $1/V_{max}$  over the appropriate sample of ELM WD binaries.

Applying the modified  $1/V_{max}$  method to the disk sample, we estimate a local space density of  $160 \text{ kpc}^{-3}$  disk ELM WD binaries using the Jurić et al. (2008) disk model, and  $300 \text{ kpc}^{-3}$  disk ELM WD binaries using the Nelemans et al. (2001) disk model. These are observed space densities, corrected only for survey completeness. We consider evolutionary time and merger time corrections in the next subsection. The factor of two difference between the two estimates is explained by the shorter thick disk radial scale length and the use of  $\text{sech}(Z)^2$  in the Nelemans et al. (2001) model, both of which cut off the effective disk volume and thus boost the local density. We consider this factor of two the uncertainty in the space density estimate. Henceforth, we adopt the Jurić et al. (2008) model-derived values in our discussion unless making comparison to AM CVn stars.

Applying the modified  $1/V_{max}$  method to the halo sample, we estimate a local space density of  $6 \text{ kpc}^{-3}$  halo ELM WD binaries using the Jurić et al. (2008) halo model. This density is 4% of the disk value, about the same percentage as the relative normalization of the halo with respect to the thick disk in the Jurić et al. (2008) models. The density ratio of disk to halo ELM WD binaries that we derive from the observations thus appears sensible given the assumed Galactic model.

### 3.2. Merger Rate of ELM WD Binaries: Reverse Approach

We now come to the crux of the problem: the merger rate of ELM WD binaries in the Milky Way. We estimate the merger rate in two ways. In this subsection, we derive a merger rate from the observed sample by correcting for the ELM WD binaries that have cooled or merged over the past Gyr. This is the approach used in Brown et al. (2011a), however we have a number advantages over our previous work. We now have orbital inclination constraints for a number of individual systems: 2 systems are eclipsing (Brown et al. 2011b; Kilic et al. 2014b), 8 have ellipsoidal variations (Kilic et al. 2011c; Hermes et al. 2012a, 2014), and many more have X-ray and/or radio observations that rule out neutron star companions (Kilic et al. 2011a, 2012, 2014b). As described above, ELM WD evolutionary models allow us to estimate the distribution of  $t_{obs}$  for each object, and the large sample size allows us to statistically constrain  $M_2$

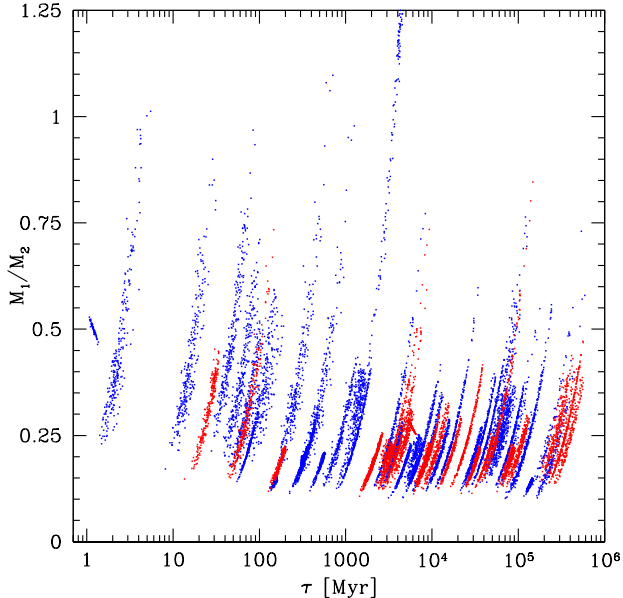


FIG. 5.— Gravitational wave merger time  $\tau$  versus mass ratio for the clean sample of ELM WD binaries. Each dot represents a Monte Carlo calculation accounting for the observational uncertainties in  $M_1$ ,  $P$ , and  $k$  plus the statistical  $M_2$  constraint given any other information (i.e. eclipses). Disk objects are blue, halo objects are red.

and thus  $\tau$ . Figure 5 plots the distribution of  $M_1/M_2$  versus  $\tau$  relevant to this discussion, colored by disk and halo classification.

Given the merger and evolutionary time of each ELM WD binary, we estimate the total number of ELM binaries that must have merged or evolved out of the sample in the last 1 Gyr. For example, J0651 has  $\tau = 1$  Myr. While it is possible that J0651 is a fluke observation, it is not the only short merger time system in our sample: we also observe ELM WD binaries with  $\tau = 2, 15,$  and  $27$  Myr. We will thus assume that the existence of one  $\tau = 1$  Myr binary implies that  $1/\tau = 1000$  such objects merged in the last 1 Gyr. In other words, we assume that ELM WD binaries are formed at a constant rate over the past Gyr. Other objects in our sample will cool out of our Survey before they merge. Mathematically, each ELM WD binary in our sample corresponds to  $N_{\text{corrected}}$  systems given by the maximum of the  $1/\tau$  and  $1/t_{\text{obs}}$  times.

Applying these corrections to the disk sample, the local space density of disk ELM WD binaries that formed in the last 1 Gyr is  $5600 \text{ kpc}^{-3}$ . As a sanity check, we compare with the local space density implied by the nearest ELM-like WD binary. WD 1242–105 is a  $0.39 M_{\odot} + 0.56 M_{\odot}$  double degenerate binary with a 0.74 Gyr merger time at a distance of 39 pc (Debes et al. 2015). Assuming that 66% – 78% of all WDs are known within 40 pc (Limoges et al. 2015), WD 1241–105 implies a local space density of  $5200 \text{ kpc}^{-3} - 6100 \text{ kpc}^{-3}$  ELM-like WD binaries, consistent with our estimate.

Finally, we integrate the total number of disk ELM WD binaries over the Galactic disk model and divide by 1 Gyr to obtain an estimated merger rate of  $3 \times 10^{-3} \text{ yr}^{-1}$ . The halo is less well constrained because the halo model is a power law instead of an exponential. If we integrate the halo model out to 100 kpc, the estimated

merger rate of halo ELM WD binaries is  $3 \times 10^{-4} \text{ yr}^{-1}$ .

The merger rate of disk ELM WDs is 75 times larger than our previous estimate in Brown et al. (2011a) for two reasons: our sample is 5 times larger than before, and we have discovered systems with order-of-magnitude faster merger times. The three disk ELM WD binaries with  $P < 0.028$  day ( $1 < \tau < 15$  Myr) contribute 90% of the corrected number of ELM WD binaries that formed in the last Gyr. By comparison, the 10 systems with  $0.042 < P < 0.08$  day ( $45 < \tau < 360$  Myr) contribute only 7% of the corrected number of disk ELM WD binaries that formed in the last Gyr. Our result is thus sensitive to the shortest orbital period systems in the sample. In the most extreme example, the merger rate drops by a factor of 2.5 if we drop the  $\tau = 1$  Myr system J0651 from the sample. Yet J0651 exists, as do the other  $P < 0.028$  day systems.

### 3.3. Merger Rate of ELM WD Binaries: Forward Approach

We estimate the merger rate of ELM WD binaries with a second approach: forward-modeling to match the observed distributions. A forward-modeling approach allows us to explore distributions instead of individual objects, and to explore our sensitivity to different input assumptions. The results remain linked to the previous estimate, however, because we normalize the model to the observed ELM WD binary space density.

#### 3.3.1. Model

The basic idea of our model is to generate ELM WD binaries over a series of time steps, evolve their orbital periods with gravitational wave radiation, and then “observe” the final distribution with the ELM WD evolutionary tracks. The most important input is the initial period distribution. It is difficult to find an initial period distribution that yields simulated observations that match the actual observations of  $P$  and  $k$ . We infer the merger rate by counting the number of simulated WD ELM binaries that remain observable compared to the number that merged over the last 1 Gyr of the simulation.

In detail, we start by adopting a Galactic star formation rate history. Solar neighborhood studies find an approximately constant (Cignoni et al. 2006) or a modestly rising (Tremblay et al. 2014) star formation rate history for the Galactic disk. Whether the star formation rate is increasing, decreasing, or constant over the last 5 Gyr makes very little difference to the simulations, however, because the ELM WD binary merger rate is dominated by those systems that form in the last Gyr in our model. We adopt a constant formation rate for simplicity. In our model, we generate 100 ELM WD binaries at every 1 Myr timestep over the 5 Gyr run of our simulations. This can also be thought of as 5,000 bursts of ELM WD binary formation spread uniformly over time.

We generate simulated ELM WD binaries by drawing values for  $M_1$ ,  $M_2$ ,  $P$ , and  $i$  as follows. We randomly draw  $M_1$  from the observed disk or halo  $M_1$  distribution, corrected for  $1/t_{\text{obs}}$  (green line in Figure 1) so that we draw ELM WD masses in the correct proportion. To match the observed  $M_1$  distribution requires that we draw more short  $t_{\text{obs}}$  ELM WDs than long  $t_{\text{obs}}$  ELM WDs.

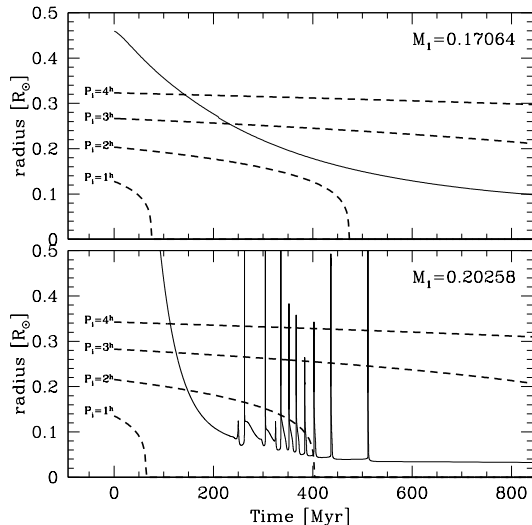


FIG. 6.— Theoretical ELM WD radius (solid line) versus time for  $0.17064 M_{\odot}$  and  $0.20258 M_{\odot}$  evolutionary tracks (Althaus et al. 2013) compared to approximate Roche lobe radii  $R_L$  (dashed lines) calculated assuming gravitational wave energy loss for  $M_2 = 0.76 M_{\odot}$  and four different initial periods  $P_i$ . Note the shell flashes present in the  $0.20258 M_{\odot}$  track and absent in the  $0.17064 M_{\odot}$  track. We start our simulated binaries at the moment when  $R_{\text{ELM}} < R_L$ , in other words, by shifting the dashed lines to the right in this plot.

We randomly draw  $M_2$  from a normal distribution with mean  $0.76 M_{\odot}$  and dispersion  $0.25 M_{\odot}$ , as described above, and impose  $0.01 M_{\odot}$  and  $3 M_{\odot}$  limits on the allowed range. We tried exploring different  $M_2$  distributions, such as the WD mass distribution observed by SDSS (Kepler et al. 2007), however this has only a 10% effect on merger times and rates because  $\tau$  is driven by orbital period (Equation 9). Limiting  $M_2$  to  $< 1.4 M_{\odot}$  also makes little difference, because  $1.4 M_{\odot}$  is  $2.6\text{-}\sigma$  from the mean and affects only 0.5% of  $M_2$  draws. After drawing  $M_2$ , we draw inclination from a random  $\sin i$  distribution.

Finally, we randomly draw  $P$  from a lognormal distribution,

$$f_P(P; \mu_P, \sigma_P^2) = \frac{1}{P\sqrt{2\pi}\sigma_P} \exp\left(-\frac{(\ln P - \mu_P)^2}{2\sigma_P^2}\right), \quad (12)$$

where  $P$  is the period,  $\mu_P$  is the lognormal mean, and  $\sigma_P$  is the standard deviation. The lower bound on  $P$  depends on the Roche lobe radius, and is thus linked to the evolutionary tracks. When we adopt  $M_1$ , we adopt a track. The Althaus et al. (2013) tracks begin at the moment the ELM WD progenitor detaches from the common envelope, which is  $P > 1$  day (or  $\tau > 300$  Gyr) (Althaus et al. 2013). The tracks are thus in conflict with the observed ELM WD binaries, which have shorter periods. Our solution is to find the earliest time in a track at which  $R_{\text{ELM}} < R_L$ , and start the calculation from there. If  $P$  is too small to be allowed at any time in a track, we note the failure and re-draw  $P$ . This approach presumes that ELM WDs are unchanged by different detachment times, but is a self-consistent way of dealing with ELM WD radii. Figure 6 illustrates the issue. In solid lines, we plot ELM WD radius versus time for two representative tracks from Althaus et al. (2013). In dashed lines, we plot the ELM WD Roche lobe radius versus time as-

suming gravitational wave energy loss for  $M_2 = 0.76 M_{\odot}$  and four different initial periods  $P_i$ . We ignore the brief excursions in  $R_{\text{ELM}}$  due to shell flashes in all of these calculations.

For each simulated binary, we start our model calculations at the time in a track when  $R_{\text{ELM}} < R_L$ . We then evolve the simulated binary forward in time with gravitational wave energy loss,

$$\frac{dP}{dt} = 7.935 \times 10^{-6} \frac{M_1 M_2}{(M_1 + M_2)^{1/3}} P^{-5/3} \quad (\text{days Myr}^{-1}) \quad (13)$$

where  $P$  is in days,  $M_1$  and  $M_2$  are in  $M_{\odot}$ , and  $dP/dt$  is in  $\text{days Myr}^{-1}$ . Every 1 Myr time step we draw additional binaries and update the orbital parameters of the old ones. We cease updating a simulated binary when its period becomes short enough that  $R_{\text{ELM}}$  from the track exceeds  $R_L$ , and we count it “merged.” We continue these calculations for 5 Gyr worth of time steps.

We consider ELM WD  $T_{\text{eff}}$  only at the end of the calculations, when we “observe” the final set of simulated binaries. For each simulated binary, we look up the ELM WD’s color given its age along its evolutionary track. Most of the simulated binaries merge or cool out of our color selection before the end of the calculations, but a subset remain observable. We evaluate our choice of input parameters by comparing the “observed” simulated distributions of  $P$  and  $k$  to the actual observations using the Anderson-Darling test (Figure 7).

### 3.3.2. Results

To explain the observed short-period binaries in the disk sample without over-producing long-period binaries requires that most ELM WD progenitors detach from the common envelope phase with  $< 1$  hr orbital periods. Figure 7 illustrates the result. The lefthand column shows three input  $P$  distributions. The righthand columns show the resulting output  $P$  and  $k$  distributions evolved by our model (in green), compared to the observed disk ELM WD binaries (in black). The first input distribution is a test case: all simulated binaries start with  $P = 0.2$  days. Such binaries will merge in a few Gyr and are observable at any end state, since  $t_{\text{obs}} \simeq \tau$ , however the simulation shows that only 1% would be seen at  $< 1$  hr periods. The second (middle) input distribution is a more realistic case: we start with the presently observed lognormal  $P$  distribution. This input distribution over-produces long-period binaries, however. Long-period binaries have tiny  $dP/dt$  and remain observable for the full length of  $t_{\text{obs}}$ . We must limit the initial number of long-period binaries to match the observed ratio of short- and long-period binaries.

The best match to the disk ELM WD binaries comes from an input lognormal distribution with mean  $\mu_P = -4$  day ( $e^{-4}$  days is about 30 min) and standard deviation  $\sigma_P = 1.5$ . We identify this match by searching over a broad grid  $-5 < \mu_P < -1$ ,  $0.5 < \sigma_P < 2.0$ , and then refining the grid around the best values. As seen in Figure 7c, the best matching input distribution is able to produce an observable number of short-period binaries without over-producing long-period binaries; 6% of the initial draws fail the Roche lobe radius test and must be re-drawn. Importantly, this model predicts that 30 disk ELM WD binaries merge in the last 1 Gyr for

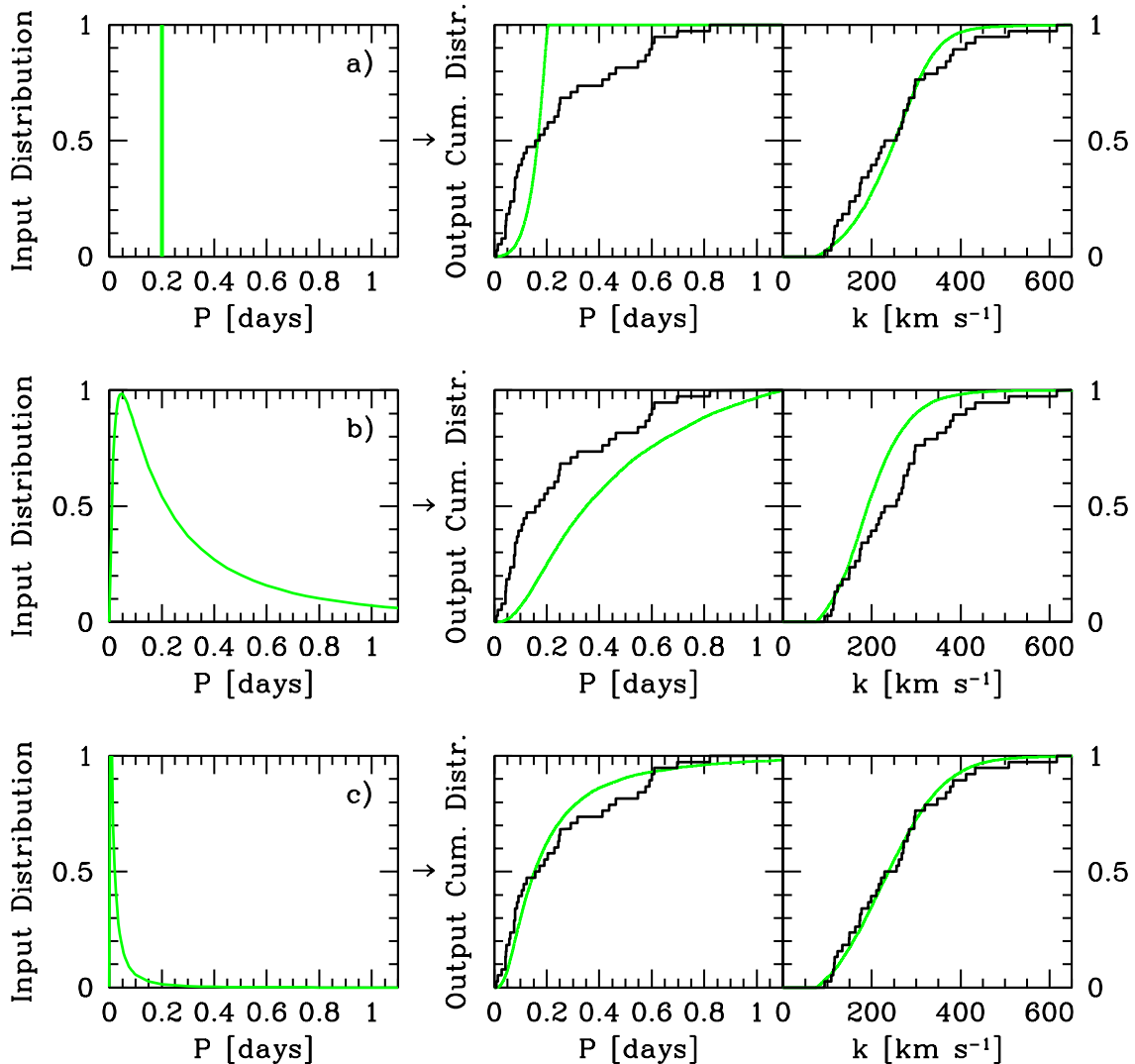


FIG. 7.— We plot three input period distributions (lefthand panels) and the resulting output  $P$  and  $k$  cumulative distributions evolved by our model (green lines, righthand panels) compared to the observations for disk ELM WD binaries (black lines). The bottom row shows the best fit, for input lognormal mean  $\mu_P = -4$  day and standard deviation  $\sigma_P = 1.5$ .

every presently observable system. Our observed disk ELM WD sample, integrated over the Jurić et al. (2008) disk model ( $0 < R < \infty, -\infty < Z < \infty$ ), implies there are about  $1 \times 10^5$  observable disk ELM WD binaries in the Galaxy. Multiplying the two numbers together and dividing by 1 Gyr yields an estimated disk ELM WD binary merger rate of  $3 \times 10^{-3} \text{ yr}^{-1}$ , in agreement with our previous estimate.

It is unclear whether a constant ELM WD binary formation rate is appropriate for the halo, however our model provides an excellent fit to the observed halo sample. Unlike the disk, the observed halo sample contains no rapidly evolving,  $M_1 > 0.21 M_\odot$  objects. The best match to the halo observations is for an input lognormal distribution with mean  $\mu_P = -2$  days (about 3 hrs) and standard deviation  $\sigma_P = 1.3$ , which results in 1.2 halo ELM WD binary mergers in the past 1 Gyr for every presently observed system. Integrating the Jurić et al. (2008) halo model to  $R = 100$  kpc implies there are

about  $6 \times 10^5$  observable ELM WD binaries throughout the halo. Multiplying the two numbers together and dividing by 1 Gyr yields an estimated halo ELM WD binary merger rate of  $7 \times 10^{-4} \text{ yr}^{-1}$ , about twice as large as our previous halo estimate.

### 3.4. Uncertainty

Our merger rate estimates rely on many assumptions, however some matter more than others. Changing the disk/halo classification of any ambiguous system alters merger rates by  $< 1\%$ , because the ambiguous systems all have long  $\tau > 200$  Myr merger times. The assumed  $M_2$  distribution (see Brown et al. 2016) changes the rates by 10%, because  $\tau$  depends only weakly on mass. The assumed star formation history also changes the rates by less than 10%.

A major source of uncertainty comes from the small number of short-period systems that drive the merger rate. In the reverse approach, three  $\tau < 15$  Myr systems

account for 90% of the disk merger rate. If we adopt  $\sqrt{N}$  as the uncertainty of observing the three binaries that dominate the result, the disk merger rate uncertainty is 60%. Bootstrap re-sampling yields the same result, a 60% variance in merger rate. The halo ELM WD binary sample has one  $\tau = 25$  Myr system that accounts for half of the halo merger rate; bootstrap re-sampling the halo sample also yields a 60% variance in merger rate. In the forward approach, bootstrap re-sampling yields a 50% variance in merger rate.

Another major source of uncertainty is the observable lifetime of ELM WDs. The choice of ELM WD evolutionary model has a 2% effect on the merger rate in the reverse approach, because  $t_{obs}$  is 20–200 times larger than  $\tau$  for the systems that drive the merger rate calculation. The forward approach is more sensitive to  $t_{obs}$ , however, because the forward approach tries to match the observed number ratio of short- and long-lived binaries. If ELM WDs have larger  $t_{obs}$  as in the Istrate et al. (2014) tracks, then the number of simulated mergers in the last Gyr is a smaller fraction of the present number of observable systems. The Istrate et al. (2014) tracks lower the merger rate by 60% in the forward approach, a difference that we adopt as the effective uncertainty of the evolutionary tracks. The larger  $t_{obs}$  times are likely explained by the lack of gravitational settling in the Istrate et al. (2014) model atmospheres, however, and so we rely on Althaus et al. (2013) tracks for all of our results.

A final source of uncertainty comes from the Galactic stellar density model used to infer the total number of ELM WD binaries in the Galaxy. Integrating the Jurić et al. (2008) and Nelemans et al. (2001) disk models  $0 < R < \infty$  and  $-\infty < Z < \infty$  yields total numbers that differ by a factor of 1.8. We adopt this factor of 1.8 as the uncertainty of the stellar density models. We can ignore this uncertainty if we compare with studies that use the identical Galactic stellar density model.

Summing the above uncertainties in quadrature, our merger rate uncertainty is 80% (a factor of 1.8) without the Galactic stellar density uncertainty, and 110% (a factor of 2.1) with it. Of course the merger rate is a lower limit to the full WD binary merger rate, because we observe only a narrow range of all WD binaries.

#### 4. DISCUSSION

Binary population synthesis models have long estimated a total Milky Way WD+WD merger rate of  $(2 - 5) \times 10^{-2} \text{ yr}^{-1}$ , most of which is predicted to be He+He and He+CO WD mergers (Iben 1990; Han 1998; Nelemans et al. 2001). The ELM WD binary (He+CO) merger rate we infer from observations is about 10% of total WD+WD merger rate, and thus consistent with the model predictions. We will now link the ELM WD binary mergers to three possible outcomes on the basis of the rates: 1) long-lived stable mass-transfer binaries, 2) explosions, and 3) mergers (Kilic et al. 2010b). We discuss the disk ELM WD binary merger rate for simplicity; adding the halo objects increase the merger rate by approximately 10%, which is less than the factor of two uncertainty.

##### 4.1. AM CVn Systems

AM CVn systems are binaries in which a CO WD is accreting helium from a companion. One formation

channel for AM CVn systems is a He+CO WD binary, in other words, an ELM WD binary (Solheim 2010). If He+CO WD binaries evolve into stable mass transfer systems, then population synthesis models predict that the AM CVn formation rate is  $6.8 \times 10^{-3} \text{ yr}^{-1}$  (Nelemans et al. 2001). If He+CO WD binaries do not evolve into stable mass transfer systems, then other formation channels dominate and the AM CVn formation rate is predicted to be  $1.1 \times 10^{-3} \text{ yr}^{-1}$  (Nelemans et al. 2001).

Observers have systematically searched for AM CVn systems in the SDSS and found 54 times fewer AM CVn systems than predicted by the optimistic population synthesis model (Roelofs et al. 2007b; Carter et al. 2013). The uncertainty in the space density of the magnitude-limited AM CVn sample is 60% (Roelofs et al. 2007b; Carter et al. 2013). The observations thus imply an AM CVn formation rate of  $(1.3 \pm 0.8) \times 10^{-4} \text{ yr}^{-1}$ .

The merger rate of disk ELM WD binaries, observed in the same footprint of sky and using the same (Nelemans et al. 2001) Galactic stellar density model parameters, is  $5 \times 10^{-3} \text{ yr}^{-1}$ , 40 times larger than the formation rate of AM CVn systems. This is the ELM WD binary merger rate using the Nelemans et al. (2001) stellar density parameters, the same parameters used in the AM CVn observational studies and the theoretical population synthesis models. The uncertainty in our ELM WD binary merger rate is a factor of 1.8. Thus the merger rate of ELM WD binaries significantly exceeds the formation rate of AM CVn at over  $3\text{-}\sigma$  confidence. Stated another way, the merger rate of ELM WD binaries is at least 8 times greater than the formation rate of AM CVn at the 99% confidence level.

##### 4.2. Underluminous Supernovae

If He+CO WD mergers instead result in explosions, they should theoretically appear as “underluminous” supernovae (e.g. Bildsten et al. 2007; Guillochon et al. 2010; Dan et al. 2011). We adopt SN 2008ha as an example of an underluminous supernova. Foley et al. (2009) estimate that SN 2008ha-like events occur at 2%–10% of the type Ia supernovae rate. From a survey of 1,000 nearby supernovae, Li et al. (2011) calculate that the type Ia supernovae rate is  $(5.4 \pm 0.1) \times 10^{-3} \text{ yr}^{-1}$  in Milky Way-like galaxies. Thus the underluminous supernovae rate in the Milky Way is approximately  $(1 - 5) \times 10^{-4} \text{ yr}^{-1}$ .

The merger rate of disk ELM WD binaries is  $3 \times 10^{-3} \text{ yr}^{-1}$  assuming Jurić et al. (2008) stellar density parameters, or 6–30 times larger than the underluminous supernovae rate. The comparison is fraught with uncertainty, however, given the different manner in which the rates are estimated. Adopting a factor of 2.1 uncertainty for the ELM WD binary merger rate, the merger rate of ELM WD binaries exceeds the underluminous supernova rate at  $2.9\text{-}\sigma$  confidence. Thus it is unlikely that all ELM WD binary mergers explode, but the conclusion is marginally significant.

##### 4.3. R Coronae Borealis Stars

R CrB stars are supergiant stars with unusual carbon-rich atmospheres, 76 of which are known in the Milky Way (Tisserand et al. 2013). One formation channel for

R CrB is the merger of He+CO WD binaries (Paczynski 1971; Webbink 1984). Recent work on R CrB formation estimates a Milky Way R CrB formation rate of  $(2 - 3) \times 10^{-3} \text{ yr}^{-1}$  (Zhang et al. 2014; Karakas et al. 2015). The merger rate of disk ELM WD binaries is statistically identical to the R CrB formation rate.

#### 4.4. He+CO WD = Unstable Mass Transfer

Our ELM WD binary merger rate is only a lower limit to the Milky Way’s full He+CO WD merger rate. We conclude that ELM WD binaries can be the progenitors of all observed AM CVn systems and possibly underluminous supernovae. The majority of ELM WD binaries, however, must go through unstable mass transfer and merge, e.g. into extreme helium stars, R CrB stars, He-rich subdwarfs, or single massive white dwarfs.

The conclusion that ELM WD binaries experience unstable mass transfer and merge is surprising given that unstable mass transfer is only assured for mass ratios  $M_1/M_2 > 2/3$ . Below that threshold there is a large region of parameter space in which the stability of mass transfer is ambiguous, and depends primarily on the strength of spin-orbit coupling (Marsh et al. 2004). Kremer et al. (2015) recently publish detailed angular momentum calculations of merging WD binaries that assumes strong spin-orbit coupling, and essentially all of their theoretical ELM WD binaries evolve into AM CVn systems. The observed rates do not match up, however.

Our observations imply that spin-orbit coupling in He+CO WD binaries is very weak. If the accretor (which spins-up due to the incoming matter stream) is unable to transfer angular momentum back to the orbit of the ELM WD on a fast enough timescale, the binary orbit shrinks, mass transfer grows and becomes unstable, and the WDs will merge (Marsh et al. 2004). An alternative explanation may lie in the initial phase of hydrogen mass transfer. Shen (2015) argues that the hydrogen mass transfer will produce a nova-like outburst that will shrink the binary orbit and drive the mass transfer rate unstable, causing a merger. Either way, our observational constraints on the ELM WD merger rate provide, for the first time, compelling evidence that mass transfer in most He+CO WD binaries is unstable.

## 5. CONCLUSION

The goal of this paper is to study the merger rate of ELM WD binaries in the Galaxy. We start by drawing a clean sample of ELM WD binaries from the ELM Survey, a spectroscopic survey of color-selected low mass WD candidates. We classify 63% of the clean sample as disk and 37% as halo on the basis of kinematics and spatial position. We derive the local space density of ELM WD binaries using the standard  $1/V_{\text{max}}$  method and a Galactic stellar density model, and then use this model to estimate that  $10^5$  ELM WD binaries presently fall in our color-selection in the Galaxy.

There are two important timescales to consider. First is the evolutionary time,  $t_{\text{obs}}$ , that an ELM WD spends cooling through our color-selection. ELM WDs with  $< 0.18 M_{\odot}$  are predicted to have long 3 Gyr evolutionary times, while ELM WDs with  $> 0.18 M_{\odot}$  experience shell flashes and cool much more quickly (Althaus et al. 2013; Istrate et al. 2014). The observed distribution of ELM WD masses, clumped around  $0.18 M_{\odot}$  with a tail

to higher mass, corroborates the predicted evolutionary timescales.

The second important timescale is the gravitational wave merger time,  $\tau$ , that is a strong function of orbital period. Observed ELM WD binaries have gravitational wave merger times that range from 1 Myr to over 100 Gyr. The shortest merger time systems drive the merger rate calculation, and this raises a concern: a recent paper about the gravitational wave properties of the  $\tau = 1$  Myr system J0651 wryly points out that “the chances of observing an eclipsing high- $f$  [short-period] binary within 1 kpc is almost zero” (Shah & Nelemans 2014). Yet J0651 and the other short-period ELM WD binaries exist. We conclude that the only way to match the observed number of short-period systems is if most of the progenitor He+CO WD binaries detach from the common envelope phase at  $P < 1$  hr periods.

We estimate the ELM WD binary merger rate in two ways. First, we correct the observed sample for the number of objects that must have merged or evolved out of the sample in the last 1 Gyr. This approach yields an ELM WD binary merger rate of  $3 \times 10^{-3} \text{ yr}^{-1}$  for the disk and a 10 times lower rate for the halo, with an uncertainty of a factor of 2. Second, we forward model to match the observed distributions. The results are insensitive to the choice of Galactic star formation rate history and secondary mass distribution, but are sensitive to the input orbital period distribution and choice of WD evolutionary tracks. The model that best describes the observations yields the same answer as before,  $3 \times 10^{-3} \text{ yr}^{-1}$ , for disk ELM WD binaries.

The estimated merger rate of disk ELM WD binaries is 40 times larger than the formation rate of AM CVn systems, marginally larger than the rate of underluminous supernovae, and statistically identical to the formation rate of R CrB stars. On this basis, we conclude that ELM WD binaries can be the progenitors of all observed AM CVn and possibly underluminous supernovae, however the majority of ELM WD binaries must merge into single massive objects.

This conclusion is unexpected given the relatively extreme mass ratios of the ELM WD binaries. And since double WD binaries with more massive WDs have mass ratios closer to one, we conclude that the majority of all double WD binaries must merge. In the future, we will explore a more detailed comparison of our observations with theoretical binary population synthesis models. The combination of merger rate, orbital period, and binary mass ratio is potentially a very powerful constraint on ELM WD binary formation channels and outcomes. Furthermore, taking the ELM Survey to its conclusion should double the sample size of ELM WD binaries, improving our constraints on the important short-period end of the distribution. There are many more interesting ELM WD binaries to be found.

This research makes use of the SAO/NASA Astrophysics Data System Bibliographic Service. We thank the referee for a timely and constructive report. This work was supported in part by the Smithsonian Institution. MK and AG gratefully acknowledge the support of the NSF and NASA under grants AST-1312678 and NNX14AF65G, respectively.

## REFERENCES

- Althaus, L. G., Miller Bertolami, M. M., & Córscico, A. H. 2013, *A&A*, 557, A19
- Andrews, J. J., Price-Whelan, A. M., & Agüeros, M. A. 2014, *ApJ*, 797, L32
- Bildsten, L., Shen, K. J., Weinberg, N. N., & Nelemans, G. 2007, *ApJ*, 662, L95
- Boffin, H. M. J. 2015, *A&A*, 575, L13
- Brown, W. R., Geller, M. J., & Kenyon, S. J. 2012a, *ApJ*, 751, 55
- Brown, W. R., Gianninas, A., Kilic, M., Kenyon, S. J., & Allende Prieto, C. 2016, *ApJ*, 818, 155
- Brown, W. R., Kilic, M., Allende Prieto, C., Gianninas, A., & Kenyon, S. J. 2013, *ApJ*, 769, 66
- Brown, W. R., Kilic, M., Allende Prieto, C., & Kenyon, S. J. 2010, *ApJ*, 723, 1072
- . 2011a, *MNRAS*, 411, L31
- . 2012b, *ApJ*, 744, 142
- Brown, W. R., Kilic, M., Hermes, J. J., et al. 2011b, *ApJ*, 737, L23
- Carter, P. J., Marsh, T. R., Steeghs, D., et al. 2013, *MNRAS*, 429, 2143
- Chiba, M. & Beers, T. C. 2000, *AJ*, 119, 2843
- Cignoni, M., Degl’Innocenti, S., Prada Moroni, P. G., & Shore, S. N. 2006, *A&A*, 459, 783
- Dan, M., Rosswog, S., Guillochon, J., & Ramirez-Ruiz, E. 2011, *ApJ*, 737, 89
- Debes, J. H., Kilic, M., Tremblay, P.-E., et al. 2015, *AJ*, 149, 176
- Eggleton, P. P. 1983, *ApJ*, 268, 368
- Foley, R. J. et al. 2009, *AJ*, 138, 376
- Gianninas, A., Kilic, M., Brown, W. R., Canton, P., & Kenyon, S. J. 2015, *ApJ*, 812, 167
- Guillochon, J., Dan, M., Ramirez-Ruiz, E., & Rosswog, S. 2010, *ApJ*, 709, L64
- Han, Z. 1998, *MNRAS*, 296, 1019
- Han, Z. & Webbink, R. F. 1999, *A&A*, 349, L17
- Heber, U., Edelmann, H., Napiwotzki, R., Altmann, M., & Scholz, R.-D. 2008, *A&A*, 483, L21
- Hermes, J. J., Brown, W. R., Kilic, M., et al. 2014, *ApJ*, 792, 39
- Hermes, J. J., Kilic, M., Brown, W. R., Montgomery, M. H., & Winget, D. E. 2012a, *ApJ*, 749, 42
- Hermes, J. J., Kilic, M., Brown, W. R., et al. 2012b, *ApJ*, 757, L21
- Iben, Jr., I. 1990, *ApJ*, 353, 215
- Istrate, A. G., Tauris, T. M., Langer, N., & Antoniadis, J. 2014, *A&A*, 571, L3
- Jurić, M. et al. 2008, *ApJ*, 673, 864
- Kaplan, D. L., Bildsten, L., & Steinfadt, J. D. R. 2012, *ApJ*, 758, 64
- Karakas, A. I., Ruitter, A. J., & Hampel, M. 2015, *ApJ*, 809, 184
- Kepler, S. O., Kleinman, S. J., Nitta, A., et al. 2007, *MNRAS*, 375, 1315
- Kilic, M., Allende Prieto, C., Brown, W. R., et al. 2010a, *ApJ*, 721, L158
- Kilic, M., Brown, W. R., Allende Prieto, C., Kenyon, S. J., & Panei, J. A. 2010b, *ApJ*, 716, 122
- Kilic, M., Brown, W. R., Allende Prieto, C., et al. 2011a, *ApJ*, 727, 3
- . 2012, *ApJ*, 751, 141
- Kilic, M., Brown, W. R., Gianninas, A., et al. 2014a, *MNRAS*, 444, L1
- Kilic, M., Brown, W. R., Hermes, J. J., et al. 2011b, *MNRAS*, 418, L157
- Kilic, M., Brown, W. R., Kenyon, S. J., et al. 2011c, *MNRAS*, 413, L101
- Kilic, M., Hermes, J. J., Gianninas, A., et al. 2014b, *MNRAS*, 438, L26
- Kraft, R. P., Mathews, J., & Greenstein, J. L. 1962, *ApJ*, 136, 312
- Kremer, K., Sepinsky, J., & Kalogera, V. 2015, *ApJ*, 806, 76
- Li, W., Chornock, R., Leaman, J., et al. 2011, *MNRAS*, 412, 1473
- Limoges, M.-M., Bergeron, P., & Lépine, S. 2015, *ApJS*, 219, 19
- Marsh, T. R., Dhillon, V. S., & Duck, S. R. 1995, *MNRAS*, 275, 828
- Marsh, T. R., Nelemans, G., & Steeghs, D. 2004, *MNRAS*, 350, 113
- Munn, J. A. et al. 2004, *AJ*, 127, 3034
- Napiwotzki, R., Karl, C. A., Nelemans, G., et al. 2007, in *ASP Conf. Ser. Vol. 372, 15th European Workshop on White Dwarfs*, ed. R. Napiwotzki & M. R. Burleigh, 387
- Nelemans, G., Portegies Zwart, S. F., Verbunt, F., & Yungelson, L. R. 2001, *A&A*, 368, 939
- Nelson, L. A., Dubeau, E., & MacCannell, K. A. 2004, *ApJ*, 616, 1124
- Paczyński, B. 1971, *Acta Astron.*, 21, 1
- Panei, J. A., Althaus, L. G., Chen, X., & Han, Z. 2007, *MNRAS*, 382, 779
- Piersanti, L., Yungelson, L. R., & Tornambé, A. 2015, *MNRAS*, 452, 2897
- Rebassa-Mansergas, A., Rybicka, M., Liu, X.-W., Han, Z., & García-Berro, E. 2015, *MNRAS*, 452, 1637
- Roelofs, G. H. A., Groot, P. J., Benedict, G. F., et al. 2007a, *ApJ*, 666, 1174
- Roelofs, G. H. A., Nelemans, G., & Groot, P. J. 2007b, *MNRAS*, 382, 685
- Sackett, P. D. 1997, *ApJ*, 483, 103
- Saio, H. & Jeffery, C. S. 2002, *MNRAS*, 333, 121
- Sarna, M. J., Ergma, E., & Gerškevič-Antipova, J. 2000, *MNRAS*, 316, 84
- Schmidt, M. 1975, *ApJ*, 202, 22
- Shah, S. & Nelemans, G. 2014, *ApJ*, 791, 76
- Shen, K. J. 2015, *ApJ*, 805, L6
- Shen, K. J. & Bildsten, L. 2009, *ApJ*, 699, 1365
- Solheim, J. 2010, *PASP*, 122, 1133
- Tisserand, P., Clayton, G. C., Welch, D. L., et al. 2013, *A&A*, 551, A77
- Tremblay, P.-E., Kalirai, J. S., Soderblom, D. R., Cignoni, M., & Cummings, J. 2014, *ApJ*, 791, 92
- Waldman, R., Sauer, D., Livne, E., et al. 2011, *ApJ*, 738, 21
- Warner, B. 1995, *Ap&SS*, 225, 249
- Webbink, R. F. 1984, *ApJ*, 277, 355
- Zhang, X., Jeffery, C. S., Chen, X., & Han, Z. 2014, *MNRAS*, 445, 660

TABLE 1  
 CLEAN SAMPLE OF ELM WD BINARIES

Object	$P$ (days)	$k$ (km s <sup>-1</sup> )	$M_1$ ( $M_\odot$ )	$M_2$ ( $M_\odot$ )	$t_{\text{obs}}$ (Gyr)	$\tau$ (Gyr)	disk
0651+2844	0.00886 ± 0.00001	616.9 ± 5.0	0.247 ± 0.015	0.49 <sup>+0.02</sup> <sub>-0.02</sub>	0.21 <sup>+0.05</sup> <sub>-0.05</sub>	0.001 <sup>+0.0001</sup> <sub>-0.0001</sub>	1
0935+4411	0.01375 ± 0.00051	198.5 ± 3.2	0.312 ± 0.019	0.75 <sup>+0.23</sup> <sub>-0.23</sub>	0.05 <sup>+0.02</sup> <sub>-0.01</sub>	0.002 <sup>+0.0008</sup> <sub>-0.0004</sub>	1
0106-1000	0.02715 ± 0.00002	395.2 ± 3.6	0.188 ± 0.011	0.57 <sup>+0.22</sup> <sub>-0.07</sub>	0.71 <sup>+0.06</sup> <sub>-0.04</sub>	0.027 <sup>+0.003</sup> <sub>-0.006</sub>	0
1630+4233	0.02766 ± 0.00004	295.9 ± 4.9	0.298 ± 0.019	0.76 <sup>+0.24</sup> <sub>-0.22</sub>	0.07 <sup>+0.03</sup> <sub>-0.02</sub>	0.015 <sup>+0.005</sup> <sub>-0.003</sub>	1
1053+5200	0.04256 ± 0.00002	264.0 ± 2.0	0.204 ± 0.012	0.75 <sup>+0.24</sup> <sub>-0.23</sub>	0.51 <sup>+0.06</sup> <sub>-0.06</sub>	0.068 <sup>+0.021</sup> <sub>-0.012</sub>	0
0056-0611	0.04338 ± 0.00002	376.9 ± 2.4	0.180 ± 0.010	0.82 <sup>+0.14</sup> <sub>-0.11</sub>	3.00 <sup>+0.00</sup> <sub>-2.17</sub>	0.076 <sup>+0.008</sup> <sub>-0.008</sub>	1
1056+6536	0.04351 ± 0.00103	267.5 ± 7.4	0.334 ± 0.016	0.76 <sup>+0.22</sup> <sub>-0.22</sub>	0.03 <sup>+0.01</sup> <sub>-0.01</sub>	0.045 <sup>+0.014</sup> <sub>-0.009</sub>	1
0923+3028	0.04495 ± 0.00049	296.0 ± 3.0	0.275 ± 0.015	0.76 <sup>+0.23</sup> <sub>-0.21</sub>	0.12 <sup>+0.03</sup> <sub>-0.03</sub>	0.059 <sup>+0.017</sup> <sub>-0.011</sub>	1
1436+5010	0.04580 ± 0.00010	347.4 ± 8.9	0.234 ± 0.013	0.78 <sup>+0.23</sup> <sub>-0.19</sub>	0.27 <sup>+0.07</sup> <sub>-0.04</sub>	0.071 <sup>+0.017</sup> <sub>-0.012</sub>	1
0825+1152	0.05819 ± 0.00001	319.4 ± 2.7	0.278 ± 0.021	0.80 <sup>+0.22</sup> <sub>-0.19</sub>	0.10 <sup>+0.07</sup> <sub>-0.03</sub>	0.113 <sup>+0.027</sup> <sub>-0.020</sub>	1
1741+6526	0.06111 ± 0.00001	508.0 ± 4.0	0.170 ± 0.010	1.17 <sup>+0.07</sup> <sub>-0.03</sub>	3	0.154 <sup>+0.004</sup> <sub>-0.006</sub>	1
0755+4906	0.06302 ± 0.00213	438.0 ± 5.0	0.184 ± 0.010	0.96 <sup>+0.16</sup> <sub>-0.10</sub>	0.78 <sup>+0.03</sup> <sub>-0.05</sub>	0.178 <sup>+0.015</sup> <sub>-0.019</sub>	0
2338-2052	0.07644 ± 0.00712	133.4 ± 7.5	0.258 ± 0.015	0.75 <sup>+0.24</sup> <sub>-0.23</sub>	0.16 <sup>+0.05</sup> <sub>-0.04</sub>	0.262 <sup>+0.087</sup> <sub>-0.050</sub>	1
2309+2603	0.07653 ± 0.00001	412.4 ± 2.7	0.176 ± 0.010	0.96 <sup>+0.16</sup> <sub>-0.10</sub>	3	0.313 <sup>+0.025</sup> <sub>-0.033</sub>	1
0849+0445	0.07870 ± 0.00010	366.9 ± 4.7	0.179 ± 0.010	0.86 <sup>+0.19</sup> <sub>-0.14</sub>	3	0.360 <sup>+0.049</sup> <sub>-0.049</sub>	1
0751-0141	0.08001 ± 0.00279	432.6 ± 2.3	0.194 ± 0.010	0.98 <sup>+0.01</sup> <sub>-0.01</sub>	0.63 <sup>+0.02</sup> <sub>-0.02</sub>	0.317 <sup>+0.003</sup> <sub>-0.004</sub>	1
2119-0018	0.08677 ± 0.00004	383.0 ± 4.0	0.159 ± 0.010	0.84 <sup>+0.14</sup> <sub>-0.05</sub>	3	0.529 <sup>+0.025</sup> <sub>-0.055</sub>	1
1234-0228	0.09143 ± 0.00400	94.0 ± 2.3	0.227 ± 0.014	0.75 <sup>+0.24</sup> <sub>-0.23</sub>	0.31 <sup>+0.08</sup> <sub>-0.06</sub>	0.476 <sup>+0.157</sup> <sub>-0.089</sub>	1
1054-2121	0.10439 ± 0.00655	261.1 ± 7.1	0.178 ± 0.011	0.77 <sup>+0.24</sup> <sub>-0.20</sub>	3.00 <sup>+0.00</sup> <sub>-2.17</sub>	0.832 <sup>+0.212</sup> <sub>-0.148</sub>	1
0745+1949	0.11240 ± 0.00833	108.7 ± 2.9	0.164 ± 0.010	0.15 <sup>+0.34</sup> <sub>-0.03</sub>	3	3.91 <sup>+0.85</sup> <sub>-2.39</sub>	1
1108+1512	0.12310 ± 0.00867	256.2 ± 3.7	0.179 ± 0.010	0.78 <sup>+0.22</sup> <sub>-0.20</sub>	3	1.27 <sup>+0.30</sup> <sub>-0.21</sub>	1
0112+1835	0.14698 ± 0.00003	295.3 ± 2.0	0.160 ± 0.010	0.74 <sup>+0.15</sup> <sub>-0.05</sub>	3	2.35 <sup>+0.13</sup> <sub>-0.30</sub>	0
1233+1602	0.15090 ± 0.00009	336.0 ± 4.0	0.169 ± 0.010	0.98 <sup>+0.16</sup> <sub>-0.09</sub>	3	1.95 <sup>+0.15</sup> <sub>-0.20</sub>	0
1130+3855	0.15652 ± 0.00001	284.0 ± 4.9	0.288 ± 0.018	0.90 <sup>+0.18</sup> <sub>-0.12</sub>	0.09 <sup>+0.04</sup> <sub>-0.03</sub>	1.40 <sup>+0.18</sup> <sub>-0.19</sub>	1
1112+1117	0.17248 ± 0.00001	116.2 ± 2.8	0.176 ± 0.010	0.75 <sup>+0.24</sup> <sub>-0.23</sub>	3	3.26 <sup>+1.03</sup> <sub>-0.60</sub>	1
1005+3550	0.17652 ± 0.00011	143.0 ± 2.3	0.168 ± 0.010	0.75 <sup>+0.24</sup> <sub>-0.23</sub>	3	3.62 <sup>+1.14</sup> <sub>-0.66</sub>	0
0818+3536	0.18315 ± 0.02110	170.0 ± 5.0	0.165 ± 0.010	0.75 <sup>+0.24</sup> <sub>-0.23</sub>	3	4.06 <sup>+1.24</sup> <sub>-0.73</sub>	0
1443+1509	0.19053 ± 0.02402	306.7 ± 3.0	0.201 ± 0.013	0.99 <sup>+0.15</sup> <sub>-0.09</sub>	0.56 <sup>+0.09</sup> <sub>-0.11</sub>	3.06 <sup>+0.27</sup> <sub>-0.32</sub>	0
1840+6423	0.19130 ± 0.00005	272.0 ± 2.0	0.182 ± 0.011	0.86 <sup>+0.19</sup> <sub>-0.14</sub>	0.84 <sup>+2.16</sup> <sub>-0.09</sub>	3.76 <sup>+0.53</sup> <sub>-0.51</sub>	1
2103-0027	0.20308 ± 0.00023	281.0 ± 3.2	0.161 ± 0.010	0.88 <sup>+0.19</sup> <sub>-0.12</sub>	3	4.87 <sup>+0.56</sup> <sub>-0.62</sub>	1
1238+1946	0.22275 ± 0.00009	258.6 ± 2.5	0.210 ± 0.011	0.87 <sup>+0.19</sup> <sub>-0.13</sub>	0.45 <sup>+0.06</sup> <sub>-0.05</sub>	4.91 <sup>+0.62</sup> <sub>-0.67</sub>	0
1249+2626	0.22906 ± 0.00112	191.6 ± 3.9	0.160 ± 0.010	0.76 <sup>+0.23</sup> <sub>-0.22</sub>	3	7.51 <sup>+2.10</sup> <sub>-1.31</sub>	1
0822+2753	0.24400 ± 0.00020	271.1 ± 9.0	0.191 ± 0.012	0.93 <sup>+0.17</sup> <sub>-0.11</sub>	0.66 <sup>+0.18</sup> <sub>-0.08</sub>	6.52 <sup>+0.64</sup> <sub>-0.78</sub>	1
1631+0605	0.24776 ± 0.00411	215.4 ± 3.4	0.162 ± 0.010	0.79 <sup>+0.23</sup> <sub>-0.19</sub>	3	8.95 <sup>+2.01</sup> <sub>-1.51</sub>	1
1526+0543	0.25039 ± 0.00001	231.9 ± 2.3	0.161 ± 0.010	0.81 <sup>+0.21</sup> <sub>-0.17</sub>	3	9.07 <sup>+1.74</sup> <sub>-1.40</sub>	0
2132+0754	0.25056 ± 0.00002	297.3 ± 3.0	0.187 ± 0.010	1.07 <sup>+0.13</sup> <sub>-0.07</sub>	0.71 <sup>+0.06</sup> <sub>-0.03</sub>	6.43 <sup>+0.34</sup> <sub>-0.53</sub>	1
1141+3850	0.25958 ± 0.00005	265.8 ± 3.5	0.177 ± 0.010	0.92 <sup>+0.17</sup> <sub>-0.11</sub>	3	8.32 <sup>+0.79</sup> <sub>-0.97</sub>	0
1630+2712	0.27646 ± 0.00002	218.0 ± 5.0	0.170 ± 0.010	0.80 <sup>+0.22</sup> <sub>-0.17</sub>	3	11.3 <sup>+2.2</sup> <sub>-1.8</sub>	0
1449+1717	0.29075 ± 0.00001	228.5 ± 3.2	0.171 ± 0.010	0.83 <sup>+0.21</sup> <sub>-0.15</sub>	3	12.5 <sup>+2.0</sup> <sub>-1.9</sub>	1
0917+4638	0.31642 ± 0.00002	148.8 ± 2.0	0.173 ± 0.010	0.75 <sup>+0.23</sup> <sub>-0.23</sub>	3	16.6 <sup>+5.1</sup> <sub>-2.9</sub>	1
0152+0749	0.32288 ± 0.00014	217.0 ± 2.0	0.169 ± 0.010	0.82 <sup>+0.21</sup> <sub>-0.16</sub>	3	16.9 <sup>+2.9</sup> <sub>-2.0</sub>	0
1422+4352	0.37930 ± 0.01123	176.0 ± 6.0	0.181 ± 0.010	0.78 <sup>+0.23</sup> <sub>-0.20</sub>	0.81 <sup>+2.19</sup> <sub>-0.01</sub>	25.2 <sup>+6.0</sup> <sub>-4.2</sub>	0
1617+1310	0.41124 ± 0.00086	210.1 ± 2.8	0.172 ± 0.010	0.85 <sup>+0.20</sup> <sub>-0.14</sub>	3	30.9 <sup>+4.4</sup> <sub>-4.4</sub>	1
1538+0252	0.41915 ± 0.00295	227.6 ± 4.9	0.168 ± 0.010	0.92 <sup>+0.17</sup> <sub>-0.11</sub>	3	31.5 <sup>+3.0</sup> <sub>-3.7</sub>	0
1439+1002	0.43741 ± 0.00169	174.0 ± 2.0	0.181 ± 0.010	0.78 <sup>+0.23</sup> <sub>-0.19</sub>	0.84 <sup>+2.16</sup> <sub>-0.05</sub>	36.8 <sup>+8.5</sup> <sub>-6.2</sub>	1
0837+6648	0.46329 ± 0.00005	150.3 ± 3.0	0.181 ± 0.010	0.76 <sup>+0.24</sup> <sub>-0.22</sub>	0.83 <sup>+2.17</sup> <sub>-0.07</sub>	43.7 <sup>+12.1</sup> <sub>-7.7</sub>	1
0940+6304	0.48438 ± 0.00001	210.4 ± 3.2	0.180 ± 0.010	0.90 <sup>+0.18</sup> <sub>-0.12</sub>	0.83 <sup>+2.17</sup> <sub>-0.01</sub>	43.9 <sup>+4.8</sup> <sub>-5.5</sub>	0
0840+1527	0.52155 ± 0.00474	84.8 ± 3.1	0.192 ± 0.010	0.75 <sup>+0.24</sup> <sub>-0.23</sub>	0.66 <sup>+0.03</sup> <sub>-0.03</sub>	57.5 <sup>+18.4</sup> <sub>-10.5</sub>	0
0802-0955	0.54687 ± 0.00455	176.5 ± 4.5	0.197 ± 0.012	0.82 <sup>+0.21</sup> <sub>-0.16</sub>	0.58 <sup>+0.10</sup> <sub>-0.09</sub>	59.7 <sup>+10.7</sup> <sub>-9.3</sub>	1
1518+1354	0.57655 ± 0.00734	112.7 ± 4.6	0.147 ± 0.018	0.75 <sup>+0.24</sup> <sub>-0.23</sub>	3	97.8 <sup>+31.3</sup> <sub>-19.7</sub>	1
2151+1614	0.59152 ± 0.00008	163.3 ± 3.1	0.181 ± 0.010	0.80 <sup>+0.22</sup> <sub>-0.19</sub>	0.82 <sup>+0.02</sup> <sub>-0.02</sub>	81.2 <sup>+17.9</sup> <sub>-13.2</sub>	1
1512+2615	0.59999 ± 0.02348	115.0 ± 4.0	0.250 ± 0.014	0.76 <sup>+0.24</sup> <sub>-0.23</sub>	0.19 <sup>+0.04</sup> <sub>-0.03</sub>	65.0 <sup>+20.3</sup> <sub>-12.1</sub>	1
1518+0658	0.60935 ± 0.00004	172.0 ± 2.0	0.224 ± 0.013	0.83 <sup>+0.20</sup> <sub>-0.15</sub>	0.34 <sup>+0.06</sup> <sub>-0.05</sub>	69.8 <sup>+11.5</sup> <sub>-10.6</sub>	1
0756+6704	0.61781 ± 0.00002	204.2 ± 1.6	0.182 ± 0.011	0.95 <sup>+0.16</sup> <sub>-0.10</sub>	0.83 <sup>+2.17</sup> <sub>-0.10</sub>	79.9 <sup>+6.9</sup> <sub>-8.7</sub>	0
1151+5858	0.66902 ± 0.00070	175.7 ± 5.9	0.186 ± 0.011	0.85 <sup>+0.19</sup> <sub>-0.15</sub>	0.74 <sup>+0.06</sup> <sub>-0.06</sub>	105 <sup>+16</sup> <sub>-15</sub>	0
0730+1703	0.69770 ± 0.05427	122.8 ± 4.3	0.182 ± 0.010	0.76 <sup>+0.24</sup> <sub>-0.22</sub>	0.81 <sup>+0.02</sup> <sub>-0.01</sub>	130 <sup>+37</sup> <sub>-23</sub>	1
0811+0225	0.82194 ± 0.00049	220.7 ± 2.5	0.179 ± 0.010	1.28 <sup>+0.10</sup> <sub>-0.05</sub>	3.00 <sup>+0.00</sup> <sub>-2.17</sub>	141 <sup>+4</sup> <sub>-7</sub>	1
1241+0633	0.95912 ± 0.00028	138.2 ± 4.8	0.199 ± 0.012	0.80 <sup>+0.22</sup> <sub>-0.18</sub>	0.57 <sup>+0.06</sup> <sub>-0.07</sub>	269 <sup>+58</sup> <sub>-45</sub>	0
2236+2232	1.01016 ± 0.00005	119.9 ± 2.0	0.186 ± 0.010	0.77 <sup>+0.23</sup> <sub>-0.21</sub>	0.75 <sup>+0.02</sup> <sub>-0.01</sub>	339 <sup>+89</sup> <sub>-59</sub>	0
0815+2309	1.07357 ± 0.00018	131.7 ± 2.6	0.199 ± 0.021	0.80 <sup>+0.22</sup> <sub>-0.19</sub>	0.67 <sup>+0.11</sup> <sub>-0.35</sub>	366 <sup>+84</sup> <sub>-66</sub>	0

 NOTE. —  $M_1$  and  $t_{\text{obs}}$  derived from Althaus et al. (2013) models.